ACS Catalysis

Research Article

pubs.acs.org/acscatalysis

Triplet Oxygen Evolution Catalyzed by a Biomimetic Oxomanganese Complex: Functional Role of the Carboxylate Buffer

Ivan Rivalta,[‡] Ke R. Yang, Gary W. Brudvig, and Victor S. Batista*

Department of Chemistry, Yale University, P.O. Box 208107, New Haven, Connecticut 06520-8107, United States

Supporting Information

ABSTRACT: Photosynthetic oxygen evolution involves water splitting into triplet oxygen, protons, and electrons, as follows: $2H_2O \rightarrow {}^3O_2 + 4e^- + 4H^+$. The reaction is catalyzed by the oxomanganese complex of photosystem II, embedded in the thylakoid membrane of green plant chloroplasts and internal membranes of cyanobacteria. Biomimetic synthetic complexes have been developed over the years, although the reactivity of most of these complexes remains to be established. Here, we report a computational study of water splitting catalyzed by the mixed-valent oxomanganese dimer $[H_2O(terpy)Mn^{III}(\mu\text{-oxo})_2Mn^{IV}(terpy)OH_2]^{3+}$ (terpy = 2,2′:6′,2″-terpyridine) in acetate buffer, with emphasis on the origin of triplet oxygen and the noninnocent role of carboxylate ligands in the underlying reaction mechanism. Our calculations suggest triplet oxygen evolution from an end-on (η^1) Mn(III)-superoxo species, which forms from a hydroperoxo intermediate generated by nucleophilic attack of substrate water onto an oxyl radical Mn(IV)−O$^\bullet$. Carboxylate groups of acetate facilitate formation of the oxyl radical by shifting the redox potential of the Mn complex upon exchange with water ligands, and catalyze the O−O bond formation by deprotonating the nucleophilic water molecule. These findings provide valuable insights on the origin of triplet oxygen and on the regulatory role of the environment surrounding the inorganic core of oxomanganese complexes during catalytic oxygen evolution.

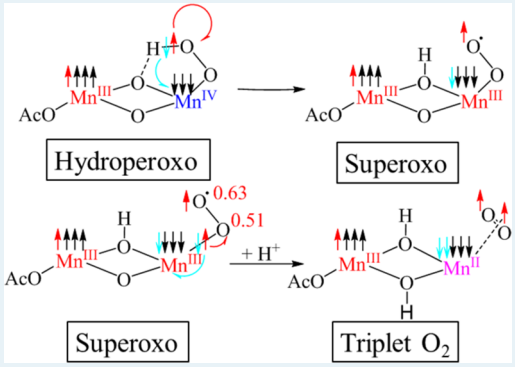

KEYWORDS: *water oxidation, O−O bond formation, biomimetic oxomanganese complexes, artificial photosynthesis, acid/base cofactors*

INTRODUCTION

Artificial photosynthetic systems mimic Nature by capturing solar light to achieve direct solar water splitting into oxygen, protons, and electrons, $2H_2O \rightarrow {}^3O_2 + 4e^- + 4H^+$. The reducing equivalents (electrons and protons) are typically used to generate chemical fuels (e.g., H_2) storing the absorbed energy in the form of chemical bonds. In Nature, water splitting is catalyzed by the oxygen-evolving complex (OEC), shown in Figure 1a, an oxomanganese cluster ligated by carboxylate groups of surrounding aspartate and glutamate side chains as well as water and imidazole groups of histidine residues in photosystem II (PSII), a complex of 20 proteins embedded in the thylakoid membrane of green plant chloroplasts and internal membranes of cyanobacteria. The water-splitting mechanism involves a multistep catalytic cycle (i.e., the "Kok cycle" proposed by Joliot and Kok[1,2]) in which, in each turnover, two water molecules bind to the cluster and produce triplet oxygen upon oxidation and deprotonation. Although the mechanism has been extensively studied, many fundamental aspects remain to be established, including the nature of deprotonations and oxidation-state transitions leading to triplet oxygen evolution and the potential functional role of the ligation environment.

Breakthroughs in X-ray crystallography have yielded the structure of the OEC cluster and its ligation scheme in PSII

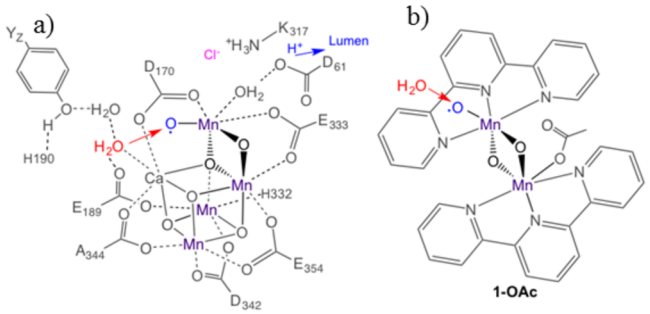

Figure 1. (a) OEC of PSII, including carboxylate groups in close contact with the inorganic core and the proposed nucleophilic attack responsible for O−O bond formation. (b) Mn-terpy dimer (**1**, terpy=2,2′:6′,2″-terpyridine) during O−O bond formation after exchanging one of its water ligands by acetate.

crystals from *Thermosynechococcus vulcanus* at 1.9 Å resolution.[3] The X-ray diffraction model provides direct evidence of terminal water ligands bound to a cuboidal oxomanganese cluster, with metal centers linked by μ-oxo bridges and ligated

Received: January 11, 2015
Revised: March 3, 2015
Published: March 5, 2015

DOI: 10.1021/acscatal.5b00048
ACS Catal. 2015, 5, 2384−2390

by carboxylate groups of surrounding amino acid residues (Figure 1a). These advances have motivated several studies addressing structure−function relations in the OEC,[4−9] including cofactors that might be involved in the deprotonation mechanism.[5] In particular, molecular dynamics (MD) simulations have addressed the functional role of chloride (Cl^-) during O_2 evolution.[5] It has been shown that Cl^- affects the configuration of the D1-Asp61 side chain, which involves a carboxylate group that might be responsible for proton abstraction from the OEC to the lumen.[5,10] In addition, density functional theory (DFT) calculations[8] have indicated that the carboxylate group of D1-Glu189 (Figure 1a) is part of a H-bond network that links the Mn cluster and the redox-active tyrosine (Y_Z). Several studies of water splitting have suggested that the O−O bond formation involves a nucleophilic attack of water to an oxyl radical Mn(IV)−O$^\bullet$ formed upon deprotonation and partial oxidation of a terminal water ligand.[11−20] Such a reaction was suggested for both PSII[11−17] and homogeneous Mn catalysts;[18−20] however, several studies that neglected the influence of carboxylate proton acceptor groups have disfavored that process because of the large energy barriers computed for O−O bond formation.[18,19,21,22] Here, for the first time, we address the influence of interactions with carboxylate groups on the underlying reaction mechanism catalyzed by a Mn-terpy complex (Figure 1b).

Several oxomanganese complexes have been proposed as biomimetic models of the OEC of PSII,[17,23−33] including the Mn terpy dimer $[H_2O(terpy)Mn(\mu\text{-}O)_2Mn(terpy)OH_2]^{3+}$ (**1**, terpy = 2,2′:6′,2″-terpyridine), in which terminal water molecules are bound to an inorganic core of high-valent Mn centers, linked by μ-oxo bridges (Figure 1b). It has been shown that **1** catalyzes water-splitting when activated by a primary oxidant both in homogeneous solutions[34,35] or immobilized in clays,[36,37] and when deposited on TiO_2 thin films;[38−40] however, the underlying catalytic mechanism remains to be established at the molecular level. We focus on the analysis of the process outlined in Figure 2 at the density functional theory (DFT) level.

METHODS

The ground state Mn−terpy dimer involves antiferromagnetic coupling between the two Mn centers in their high-spin states. Rigorous description of antiferromagnetic states in principle requires multideterminant wave functions.[41] Only multi-reference methods, such as complete active space self-consistent field (CASSCF)[42,43] or second-order perturbation theory based on CASSCF wave function (CASPT2),[44,45] are formally able to describe the antiferromagnetic coupling states; however, the size of our system prevents the application of those methods. Therefore, we limit our analysis of the antiferromagnetic ground states to spin-polarized calculations using the broken symmetry (BS) method in which the α and β electronic densities are localized on different metal centers.[46]

Quantum mechanical electronic structure calculations were carried out at the DFT level using Gaussian09.[47] The hybrid exchange-correlation functional B3LYP[48,49] was used because of its capabilities in characterizing proton-coupled electron transfer in biomimetic oxomanganese complexes.[30] The geometry optimization was performed with a mixed basis set, including the Los Alamos LanL2DZ pseudopotential to account for a nonrelativistic description of electron−core potentials and the LanL2DZ basis set for the Mn(III) and

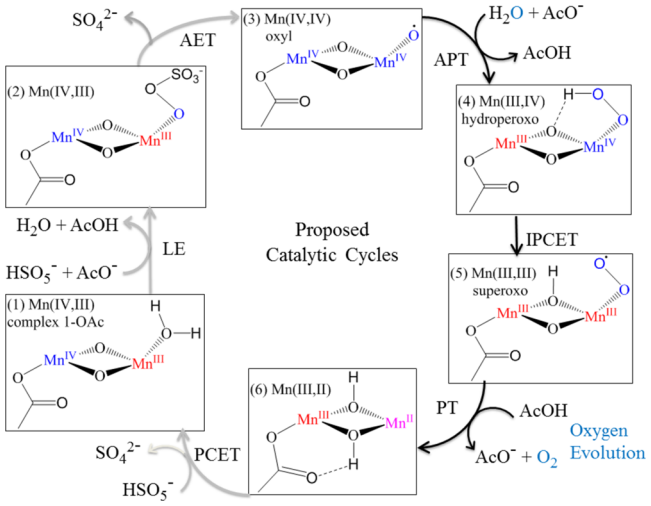

Figure 2. Proposed catalytic cycle of water oxidation catalyzed by complex **1** in acetate/acetic acid buffer, using oxone (HSO_5^-) as the primary oxidant. For simplicity, terpy ligands are omitted. The present computational study focuses on the reaction steps shown in black. (abbreviations: LE, ligand exchange; AET, concerted atom−electron transfer; APT, concerted atom-proton transfer; IPCET, intramolecular proton-coupled electron transfer; PT, proton transfer; PCET, proton-coupled electron transfer).

Mn(IV) centers,[50] the 6-31G(d) basis set for O atoms to include polarization functions for μ-oxo species, the 6-31G basis set for N atoms coordinated to Mn centers, and the 3-21G basis sets for the rest of the (C, H) atoms in the bulky ligands. For each optimized stationary point, vibrational analysis has been performed to determine its character, minimum, or saddle point (for which intrinsic reaction coordinate (IRC) analysis were also carried out, see Figures S1−S7) and to calculate the thermal correction to the Gibbs free energy. Single-point energy calculations based on Dunning's correlation-consistent triple-ζ basis set cc-pVTZ(-f),[51−53] including a double set of polarization functions, were performed upon optimized geometries to obtain accurate total energies. The methods implemented in the calculation of redox potentials and pK_a's of oxomanganese complexes have already been described in our previous works, showing excellent agreement between calculated and experimental data.[30,31]

RESULTS

The proposed catalytic cycle is shown in Figure 2. The process starts in state 1 with the acetate-substituted complex **1** because there is evidence from DFT calculations and cyclic voltammetry[30] as well as EPR studies[54] that one of the two terminal water ligands spontaneously exchanges with acetate in acetic acid/acetate buffer solutions. The other water ligand could exchange with peroxomonosulfate (HSO_5^-) during the 1 → 2 transition. Transition 2 → 3 forms the oxyl radical species Mn(IV)−O$^\bullet$ in the rate-limiting step, with an energy barrier of 15−17 kcal/mol, which is consistent with the experimental turnover number of 0.67 s^{-1}.[18,35]

Scheme 1 shows that the Mn(IV)−O$^\bullet$ radical is generated by O−O bond cleavage in the AcO−Mn(IV)−$(\mu\text{-}O)_2$−Mn(III)−$OOSO_3^-$ complex. The unpaired electron on the O atom in the Mn(IV)−O$^\bullet$ radical could have a spin either parallel or antiparallel to the three spins on the adjacent Mn(IV) center. We will call the two states parallel-spin (PS) and antiparallel-spin (AS) Mn(IV)−O$^\bullet$ radicals in the following discussion.

DOI: 10.1021/acscatal.5b00048
ACS Catal. 2015, 5, 2384−2390

Scheme 1. Possible Mechanisms of the Generation of the Mn(IV)−O• Oxyl Radical and Electron Transfer to Mn(IV) Centers during Catalytic O−O Bond Formation, Including Parallel-Spin and Antiparallel-Spin Mn(IV)−O• Radicals

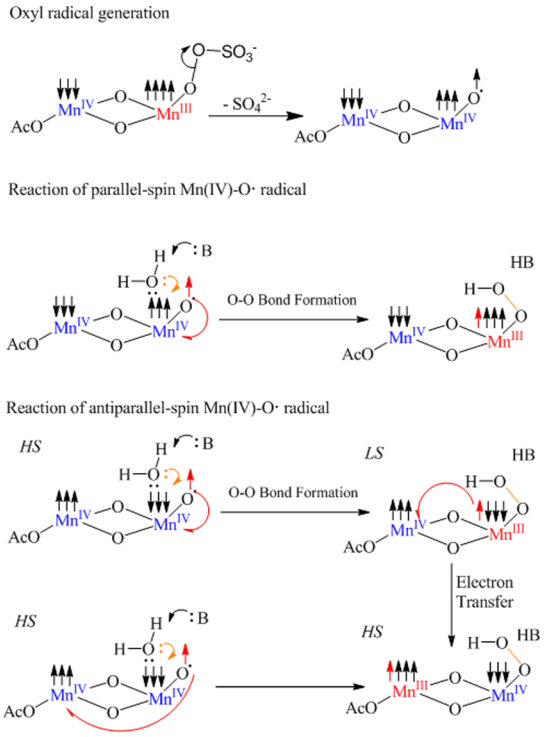

When the spin is conserved, the parallel-spin Mn(IV)−O• radical would be generated by O−O bond cleavage because the unpaired electron on O atom comes from the adjacent Mn(III) center, which is parallel to the three spins on the resulting Mn(IV) center. However, the antiparallel-spin Mn(IV)−O• radical (with a spin on the O atom antiparallel to the three spins on the adjacent Mn(IV) center) is energetically more stable. Therefore, the following reactions would proceed from the antiparallel spin oxyl radical when spin crossing is allowed by the spin−orbital coupling. For comparison, we analyze both possibilities.

Scheme 1 shows that the O−O bond is formed during the (3) → (4) transition, involving a nucleophilic attack on the Mn(IV)−O• radical by a water molecule activated by a base (B) (e.g., acetate). The nucleophilic attack on the parallel-spin Mn(IV)−O• radical yields the hydroperoxo complex, AcO−Mn(IV)−(μ-O)$_2$−Mn(III)−OOH upon forming the O−O bond and transferring an electron from the oxyl to the adjacent Mn(IV) center. The antiparallel-spin Mn(IV)−O• radical, however, can react by concerted O−O bond formation and electron transfer to the distal Mn(IV) center. An alternative mechanism proceeds in a stepwise fashion. First, the O−O bond is formed via the nucleophilic attack of a water molecule assisted by a base onto the oxyl radical. The unpaired alpha electron on the O atom is transferred into the adjacent Mn(IV) center, forming a low-spin triplet Mn(III) ion, and then the alpha electron is transferred to the distal Mn(IV) center to form the more stable AcO−Mn(III)−(μ-O)$_2$−Mn(IV)−OOH species with both Mn centers in high-spin states. Both mechanisms are effectively the same when the low-spin Mn(III) intermediate becomes unstable.

For both types of intermediates, including the parallel-spin and antiparallel-spin Mn(IV)−O• radical species, the O−O bond formation is assisted by a base (B) that extracts a proton from the substrate water molecule during the nucleophilic attack. Therefore, the nature of the base has a critical effect on the reaction free energy profile. The resulting hydroperoxo species AcO−Mn(III)−(μ-O)$_2$−Mn(IV)−OOH, or AcO−Mn(IV)−(μ-O)$_2$−Mn(III)−OOH, spontaneously rearranges to form the intermediate AcO−Mn(III)−(μ-O, μ-OH)−Mn(III)−OO• (formally, a (η^1) Mn(IV)−O_2^- superoxo) through intramolecular proton-coupled electron transfer (IPCET). The subsequent decomposition of the superoxo intermediate Mn(III)−OO•, in the 5 → 6 transition, releases triplet oxygen. The complex is left in the AcO−Mn(III)−(μ-OH)$_2$−Mn(II) state and quickly completes the cycle to regenerate the Mn(IV)−Mn(III) state by reacting with the primary oxidant.[35]

Figure 3 compares experimental and calculated (DFT) Pourbaix diagrams giving the pH dependence of the (III,IV) → (IV,IV) redox potential for **1** in the presence or absence of acetate. These results clearly show that the pH-dependent cyclic voltammetry (CV) experiments and DFT calculations are consistent with the exchange of H_2O by acetate ligated to Mn(IV) in complex **1**.[28,31] Acetate stabilizes the oxidized form of the complex and, therefore, decreases the potential for oxidation of Mn(III) by as much as 90−220 mV throughout the complete range of pH. In addition, acetate binding affects the pK_a of the terminal water and, therefore, reduces the pH range for proton-coupled electron transfer (PCET) in which the potential changes linearly with 60 mV per unit of pH. These results show that carboxylate ligands bound to Mn, as in the OEC of PSII, facilitate oxidation of the oxomanganese complex and modulate the pH range for PCET.

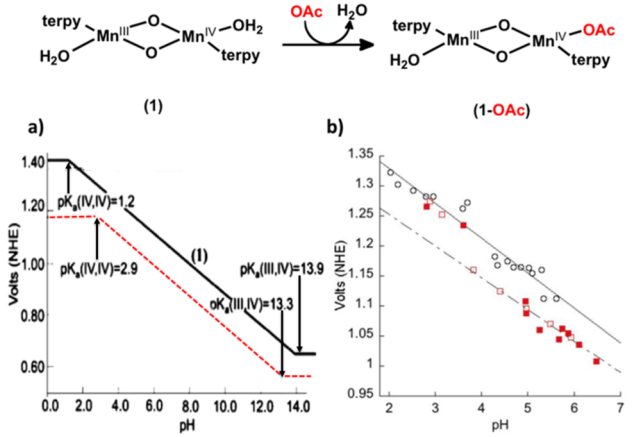

Figure 3. (a) Pourbaix diagrams for complexes **1** and **1-OAc**, obtained from free energy calculations of redox potentials and pK_a's at the DFT B3LYP/cc-pVTZ(-f) level of theory, in aqueous solutions (black solid line) and with acetate binding (red dashed line). (b) Experimental potentials for oxidation of **1** vs pH, showing **1** in unbuffered aqueous solution (open black circles), **1** in an aqueous solution buffered with 50 mM acetate (open red squares, **1-OAc**) and **1** in an aqueous solution buffered with 50 mM pyridine (solid red squares), as reported in ref 31 (panel a) and ref 28 (panel b).

Figure 4 shows the DFT/B3LYP free energy profiles of the O−O bond-forming reaction during the water nucleophilic attack on the Mn(IV)−O• radical, assisted by a μ-oxo bridge (Figure 4, upper panel) or a buffer acetate molecule (Figure 4, lower panel). Both parallel-spin and antiparallel-spin Mn(IV)−

DOI: 10.1021/acscatal.5b00048
ACS Catal. 2015, 5, 2384−2390

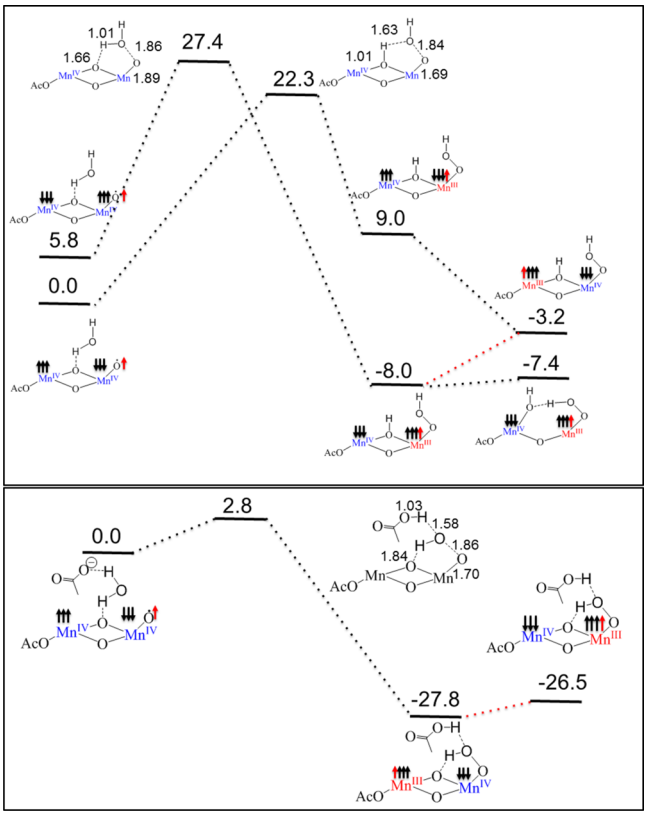

Figure 4. DFT/B3LYP free energy surfaces (in kcal/mol) of O−O bond formation catalyzed by complex **1-OAc** in the presence (bottom panel) and the absence (top panel) of an acetate molecule in solution. The Mn(IV)−O• radical of the Mn(IV)−Mn(IV) dimer undergoes nucleophilic attack by water, producing the hydroperoxo Mn(III)−Mn(IV) species via concerted O atom−proton transfer (APT). Terpy ligands are omitted for clarity, and key bond lengths in transition states are shown in Å. Alpha and beta spins on Mn center are represented by up and down arrows.

O• radicals were considered for the case of the μ-oxo bridge acting as a base. The antiparallel-spin Mn(IV)−O• radical with the spin on the O radical antiparallel to the three beta spins on its adjacent Mn(IV) center is 5.8 kcal/mol more stable than the parallel-spin Mn(IV)−O• radical. When the Mn(IV)−Mn(IV) μ-oxo bridge is the proton acceptor, the activation free energies for the nucleophilic attack of a water molecule are 22.3 and 21.6 kcal/mol for the antiparallel-spin and parallel-spin Mn(IV)−O• radicals, respectively. These results are in agreement with a previous theoretical analysis based on a reduced model of complex **1**.[18] Such large activation barriers, however, are inconsistent with the O_2-evolution reaction rate observed experimentally.[35] In contrast, the acetate-assisted O−O bond formation via the nucleophilic attack of a water molecule on the antiparallel-spin Mn(IV)−O• radical has a much lower activation free energy of only 2.8 kcal/mol, showing the dramatic effect of the environment on the reaction free energy profile, which facilitates the O−O bond formation and makes the oxyl radical formation the rate-limiting step of the reaction. With acetate, the parallel-spin Mn(IV)−O• radical is 4.2 kcal/mol less stable than the antiparallel-spin Mn(IV)−O• radical, comparable to the 5.8 kcal/mol energy difference in the absence of acetate. Because the transition state of the acetate-assisted nucleophilic attack of water on the antiparallel-spin Mn(IV)−O• radical is 1.4 kcal/mol more stable than the reactant complex of parallel-spin Mn(IV)−O• radical, the reaction of the parallel-spin Mn(IV)−O• radical with water in the presence of acetate is not considered any further.

The key bond lengths of the transition states for the nucleophilic attack of water on the antiparallel-spin Mn(IV)−O• radical shown in Figure 4 suggest that a proton of the substrate water molecule is already transferred to the base at the transition state, with $O_{\mu\text{-oxo}}$−H_W and $O_{acetate}$−H_W distances of 1.01 and 1.03 Å. The length of the partially formed O_W−O_{oxyl} bond is similar in both cases, with 1.84 and 1.86 Å for the μ-oxo bridge and acetate acting as the proton acceptor, suggesting that the transition states in the base-assisted nucleophilic attack of a water molecule on the antiparallel-spin Mn(IV)−O• radical are quite similar, with one of the protons of the substrate water molecule transferred to the base and the O_W−O_{oxyl} bond length at ∼1.8 Å.

The activation barrier of base-assisted O−O bond formation depends on the proton-accepting ability of the base. The calculated pK_a of the μ-oxo bridge in the Mn(IV)−Mn(IV)−O• species (pK_a < 0) is similar to that of the hydronium ion (pK_a = −1.74),[55] lower than that in the Mn(IV)−Mn(IV) dimer with the 2,2′-bipyridyl ligand (pK_a = 2.3)[28,31] and much lower than that of acetic acid (pK_a = 4.75). A lower pK_a of the conjugate acid corresponds to a lower proton-accepting ability of the base, with acetate being a better proton acceptor than Mn(IV)−Mn(IV) μ-oxo bridges. These results rationalize the significant decrease in activation barrier for the acetate-assisted O−O bond formation, indicating that buffer proton acceptor centers play a crucial role during catalytic water oxidation, a kinetic effect that has been previously observed for O−O bond formation in Ru single-site water oxidation catalysis[56] and for base-assisted proton−electron transfer reactions in tyrosine oxidation.[57] Notably, the inability of water to be an efficient acceptor in PCET reactions has also been observed in PCET pathways of homogeneous Co and Os complexes,[58,59] with buffer bases, including acetate,[59] being quite effective for triggering concerted PCET pathways.

Without the presence of effective proton acceptors such as acetate, the Mn(IV)−Mn(IV) μ-oxo bridge functions as a base to facilitate O−O bond formation. For the antiparallel-spin Mn(IV)−O• radical, a transient species, namely, AcO−Mn(IV)−(μ-O, μ-OH)−Mn(III)−OOH is formed with three beta electrons and one alpha electron in the Mn(III) center after passing the transition state. The alpha electron in the adjacent Mn(III) center transfers to the distal Mn(IV) center, resulting in the AcO−Mn(III)−(μ-O, μ-OH)−Mn(IV)−OOH complex with both Mn centers in high-spin states. This complex may undergo a spin-flip to form the more stable AcO−Mn(IV)−(μ-O, μ-OH)−Mn(III)−OOH species, which is 4.8 kcal/mol more stable and is formed by nucleophilic attack of water to the parallel-spin Mn(IV)−O• radical. The AcO−Mn(IV)−(μ-O, μ-OH)−Mn(III)−OOH species can undergo Mn(III)−(μ-)OH bond breaking to disrupt the $Mn_2(\mu\text{-O})_2$ core, thus deactivating the Mn catalyst with a slight increase in the free energy of 0.6 kcal/mol. This result suggests that the presence of the acetate buffer in solution in effect stabilizes the dimeric form of the Mn catalyst and avoids formation of labile Mn(IV)−Mn(III) intermediates containing μ-hydroxo bridges. With acetate, we could not locate an intermediate with a low-spin Mn(III) center. By following the reaction path of the nucleophilic attack of water onto the antiparallel-spin Mn(IV)−O• radical, the potential energy reaches a plateau corresponding to the AcO−Mn(IV)−$(\mu\text{-O})_2$−Mn(III)−OOH···HOAc com-

DOI: 10.1021/acscatal.5b00048
ACS Catal. 2015, 5, 2384−2390

plex after the transition state (see Figure S4). The potential energy further decreases until a minimum corresponding to AcO−Mn(III)−(μ-O)$_2$−Mn(IV)−OOH···HOAc, with both Mn centers in high-spin states. With the assistance of acetate, the reaction of antiparallel-spin Mn(IV)−O$^\bullet$ radical with water corresponds to a concerted O−O bond formation and electron transfer, as shown in Scheme 1.

Figure 5 shows the free energy profiles of triplet oxygen evolution via the AcO−Mn(III)−(μ-O, μ-OH)−Mn(III)−OO$^\bullet$

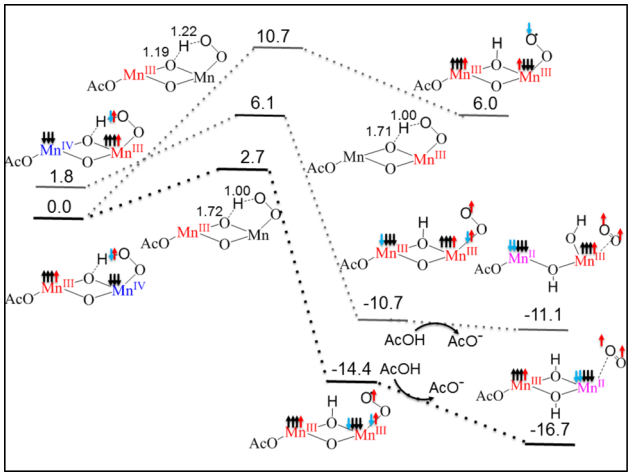

Figure 5. DFT/B3LYP free energy surfaces (in kcal/mol) for O_2 evolution catalyzed by complex **1-OAc**. The hydroperoxo Mn(III)−Mn(IV)−OOH and Mn(IV)−Mn(III)−OOH species undergo IPCET, forming the AcO−Mn(III)−(μ-OH,μ-O)−Mn(III)−OO$^\bullet$ superoxo intermediate. The Mn(III)−OO$^\bullet$ bond dissociation and electron transfer to the Mn(III) center are coupled with protonation of the μ-oxo bridge, generating triplet O_2. Terpy ligands are omitted for clarity, and key bond lengths in transitions states are shown in angstroms. Alpha and beta spins on the Mn center are represented by up and down arrows.

intermediate. The complex AcO−Mn(III)−(μ-O)$_2$−Mn(IV)−OOH, formed by acetate-assisted nucleophilic attack of the water molecule to the antiparallel-spin Mn(IV)−O$^\bullet$ radical, is 1.8 kcal/mol more stable than the AcO−Mn(IV)−(μ-O)$_2$−Mn(III)−OOH complex that is formed by acetate-assisted nucleophilic attack of the water molecule to the parallel-spin Mn(IV)−O$^\bullet$ radical. The radical AcO−Mn(III)−(μ-O, μ-OH)−Mn(III)−OO$^\bullet$ is formed by IPCET, in which the proton is transferred to one of the μ-oxo bridges and a beta electron is transferred to the adjacent Mn(IV), resulting in the Mn(III)−OO$^\bullet$ radical with an alpha spin on the O−O$^\bullet$ radical antiparallel to the four beta spins on the adjacent Mn(III) center. The activation free energy is calculated to be only 2.7 kcal/mol, very small when compared with that of O−O bond formation assisted by the Mn(IV)−Mn(IV) μ-oxo bridge (22.3 kcal/mol). This difference is due to the presence of an intramolecular H-bond between the hydroperoxo group and the proton acceptor Mn(IV)−Mn(III) μ-oxo bridge that facilitates proton abstraction from the hydroperoxo moiety (Figure 5) and to the fact that the proton accepting ability of a Mn(IV)−Mn(III) μ-oxo bridge ($pK_a \approx 2.0$)[28,30] is higher than that of the Mn(IV)−Mn(IV) μ-oxo bridge ($pK_a < 0$). Another channel is also possible for intramolecular proton-coupled electron transfer, which has an activation free energy of 10.7 kcal/mol, leading to a high-energy triplet Mn(III) ion. This channel is not relevant to triplet oxygen evolution.

The complex AcO−Mn(IV)−(μ-O)$_2$−Mn(III)−OOH, formed through reaction of the parallel-spin Mn(IV)−O$^\bullet$ radical, can also undergo intramolecular PCET to form the AcO−Mn(III)−(μ-O, μ-OH)−Mn(III)−OO$^\bullet$ radical (formally, a Mn(IV)−O_2^- superoxo intermediate) with a small activation barrier of 4.3 kcal/mol. The resulting Mn(III)−OO$^\bullet$ radical has an alpha spin of O−O$^\bullet$ parallel to four alpha spins on the adjacent Mn(III) center. This complex can also be protonated to form the AcO−Mn(III)−(μ-OH)$_2$−Mn(III)−OO$^\bullet$ species and to release O_2.

The O−O bond distances and O−O stretching frequencies in the parallel-spin and antiparallel-spin Mn(III)-superoxo complexes are 1.32 Å and 1219.2 cm^{-1}, and 1.31 Å and 1225.8 cm^{-1}, respectively, falling in the superoxide category of metal−dioxygen complexes.[60] Atomic spin densities determined from the Mulliken population analysis indicate that the electron spin density is equally distributed between the two O atoms in the π^* antibonding orbital of the O_2 fragment. Scheme 2 shows that triplet oxygen is formed upon protonation

Scheme 2. Triplet Oxygen Evolution via Formation of a Mn(III)-Superoxo Species[a]

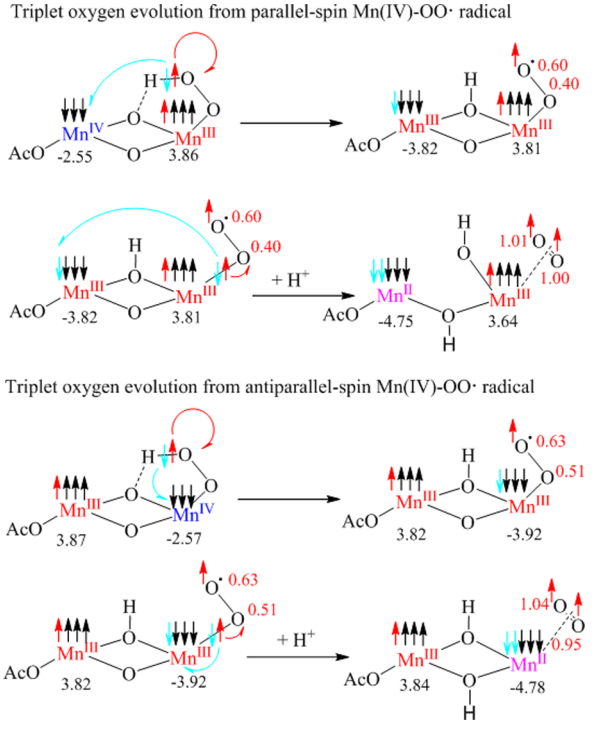

[a]Atomic spin densities calculated from Mulliken population analysis are shown for Mn and O atoms relevant to O_2 evolution.

of the antiparallel-spin Mn(III)−OO$^\bullet$ superoxo through a barrier-less bond-breaking process concerted with electron transfer of an alpha electron to the π^* antibonding orbital of O_2 and a beta electron to the d orbital of the adjacent Mn(III) center. As shown in Figure 5, both the Mn(III)−OO$^\bullet$ bond dissociation and electron transfer to the Mn(III) center are coupled to protonation of the second μ-oxo bridge, giving rise to the formation of the AcO−Mn(III)−(μ-OH)$_2$−Mn(II) complex and triplet oxygen evolution. The proton used for protonation of the Mn(III)−Mn(III) μ-oxo bridge can be supplied by a buffer acetic acid molecule, with regeneration of

DOI: 10.1021/acscatal.5b00048
ACS Catal. 2015, 5, 2384−2390

the acetate molecule that would assist the O−O bond formation during the next catalytic cycle.

The evolution of triplet oxygen from the parallel-spin Mn(III)−OO$^{\bullet}$ superoxo requires cleavage of the Mn(III)−OO$^{\bullet}$ bond and transfer of a beta electron to the distal Mn(III) center, thus reducing the distal Mn(III) to Mn(II). However, Mn(II) prefers to have a coordination sphere of five ligands, rather than six. Therefore, the $Mn_2(\mu\text{-}O)_2$ core in the catalyst is disrupted. To stabilize the $Mn_2(\mu\text{-}O)_2$ core, the alpha electron from the Mn(III)−OO$^{\bullet}$ bond needs to be injected into the adjacent Mn center while the beta electron is transferred to the O_2 molecule, forming a singlet oxygen instead of a triplet oxygen (Scheme 2). That pathway would be inconsistent with experimental observations, suggesting that although the parallel-spin Mn(IV)−O$^{\bullet}$ radical is generated through a spin-conserving O−O bond cleavage in the complex AcO−Mn(IV)−$(\mu\text{-}O)_2$−Mn(III)−$OOSO_3^-$, the following reactions proceed from the more stable antiparallel-spin Mn(IV)−O$^{\bullet}$ radical.

CONCLUSIONS

We have computationally examined the origin of triplet oxygen evolution from the nucleophilic attack of substrate water onto the Mn(IV)−O$^{\bullet}$ radical of the Mn−terpyridine dimer, a functional model of the oxygen-evolving complex (OEC) of photosystem II (PSII). Both the parallel-spin and antiparallel-spin Mn(IV)−O$^{\bullet}$ radical have been considered, with emphasis on the regulatory role of the acetate buffer in the underlying reaction mechanism. Our results suggest that the water nucleophilic attack proceeds through a base-assisted O−O bond-formation reaction, followed by an intramolecular proton-coupled electron transfer that produces a formal end-on (η^1) Mn(IV)-superoxo (O_2^-) intermediate in the form of the Mn(III)−OO$^{\bullet}$ radical that readily generates triplet oxygen without a significant activation barrier.

During the nucleophilic attack, proton transfer to a carboxylate group of the acetate buffer decreases the activation barrier of the O−O bond formation step by ∼20 kcal/mol, with respect to the analogous process in which the proton is transferred to a μ-oxo bridge of the complex. The presence of the acetate buffer in solution thus expedites the nucleophilic attack and stabilizes the Mn catalyst by avoiding formation of Mn(III)−Mn(IV) intermediates containing protonated μ-oxo bridges. Moreover, acetate exchanges with a water ligand and reduces the potential for oxidation of the complex by 100−200 mV during formation of the oxyl radical. These results provide fundamental insights into the functional role of the complex ligation environment, which are expected to have important implications for understanding water-splitting in photosystem II and other biomimetic catalysts in which carboxylate groups might play similar functional roles as acid/base and redox cofactors.

ASSOCIATED CONTENT

Supporting Information

The following file is available free of charge on the ACS Publications website at DOI: 10.1021/acscatal.5b00048.

Absolute and relative energies, geometries and spin densities of all stationary points and intrinsic reaction coordinate (IRC) analysis of all transition states (PDF)

AUTHOR INFORMATION

Corresponding Author

*E-mail: victor.batista@yale.edu.

Present Address

‡(I.R.) Université de Lyon, CNRS, Institut de Chimie de Lyon, École Normale Supérieure de Lyon, 46 Allée d'Italie, F-69364 Lyon Cedex 07, France.

Notes

The authors declare no competing financial interest.

ACKNOWLEDGMENTS

V.S.B. acknowledges computing resources from NERSC and financial support as part of the Argonne-Northwestern Solar Energy Research (ANSER) Center, an Energy Frontier Research Center funded by the U.S. Department of Energy, Office of Science, Office of Basic Energy Sciences under Award No. DE-SC0001059. G.W.B. acknowledges support for experimental work from the Division of Chemical Sciences, Geosciences, and Biosciences, Office of Basic Energy Sciences, U.S. Department of Energy (DE-FG02-05ER15646).

REFERENCES

(1) Joliot, P.; Barbieri, G.; Chabaud, R. *Photochem. Photobiol.* **1969**, *10*, 309−329.
(2) Kok, B.; Forbush, B.; McGloin, M. *Photochem. Photobiol.* **1970**, *11*, 457−475.
(3) Umena, Y.; Kawakami, K.; Shen, J.-R.; Kamiya, N. *Nature* **2011**, *473*, 55−60.
(4) Luber, S.; Rivalta, I.; Umena, Y.; Kawakami, K.; Shen, J.-R.; Kamiya, N.; Brudvig, G. W.; Batista, V. S. *Biochemstry* **2011**, *50*, 6308−6311.
(5) Rivalta, I.; Amin, M.; Luber, S.; Vassiliev, S.; Pokhrel, R.; Umena, Y.; Kawakami, K.; Shen, J.-R.; Kamiya, N.; Bruce, D.; Brudvig, G. W.; Gunner, M. R.; Batista, V. S. *Biochemistry* **2011**, *50*, 6312−6315.
(6) Ames, W.; Pantazis, D. A.; Krewald, V.; Cox, N.; Messinger, J.; Lubitz, W.; Neese, F. *J. Am. Chem. Soc.* **2011**, *133*, 19743−19757.
(7) Yamanaka, S.; Isobe, H.; Kanda, K.; Saito, T.; Umena, Y.; Kawakami, K.; Shen, J. R.; Kamiya, N.; Okumura, M.; Nakamura, H.; Yamaguchi, K. *Chem. Phys. Lett.* **2011**, *511*, 138−145.
(8) Saito, K.; Shen, J.-R.; Ishida, T.; Ishikita, H. *Biochemistry* **2011**, *50*, 9836−9844.
(9) Askerka, M.; Wang, J.; Brudvig, G. W.; Batista, V. S. *Biochemistry* **2014**, *53*, 6860−6862.
(10) Dilbeck, P. L.; Hwang, H. J.; Zaharieva, I.; Gerencser, L.; Dau, H.; Burnap, R. L. *Biochemistry* **2012**, *51*, 1079−1091.
(11) Pecoraro, V. L.; Baldwin, M. J.; Caudle, M. T.; Hsieh, W. Y.; Law, N. A. *Pure Appl. Chem.* **1998**, *70*, 925−929.
(12) Ferreira, K. N.; Iverson, T. M.; Maghlaoui, K.; Barber, J.; Iwata, S. *Science* **2004**, *303*, 1831−1838.
(13) Limburg, J.; Szalai, V. A.; Brudvig, G. W. *J. Chem. Soc., Dalton Trans.* **1999**, 1353−1361.
(14) Vrettos, J. S.; Limburg, J.; Brudvig, G. W. *Biochim. Biophys. Acta, Bioenerg.* **2001**, *1503*, 229−245.
(15) Messinger, J.; Badger, M.; Wydrzynski, T. *Proc. Natl. Acad. Sci. U.S.A.* **1995**, *92*, 3209−3213.
(16) Sproviero, E. M.; Gascon, J. A.; McEvoy, J. P.; Brudvig, G. W.; Batista, V. S. *J. Am. Chem. Soc.* **2008**, *130*, 3428−3442.
(17) Sproviero, E. M.; Gascon, J. A.; McEvoy, J. P.; Brudvig, G. W.; Batista, V. S. *Coord. Chem. Rev.* **2008**, *252*, 395−415.
(18) Lundberg, M.; Blomberg, M. R. A.; Siegbahn, P. E. M. *Inorg. Chem.* **2004**, *43*, 264−274.
(19) Lundberg, M.; Siegbahn, P. E. M. *Chem. Phys. Lett.* **2005**, *401*, 347−351.
(20) Sameera, W. M. C.; McKenzie, C. J.; McGrady, J. E. *Dalton Trans.* **2011**, *40*, 3859−3870.
(21) Siegbahn, P. E. M. *Inorg. Chem.* **2008**, *47*, 1779−1786.

DOI: 10.1021/acscatal.5b00048
ACS Catal. 2015, 5, 2384−2390

(22) Siegbahn, P. E. M. *Chem.—Eur. J.* **2008**, *14*, 8290−8302.
(23) Ruettinger, W.; Yagi, M.; Wolf, K.; Bernasek, S.; Dismukes, G. C. *J. Am. Chem. Soc.* **2000**, *122*, 10353−10357.
(24) Poluektov, O.; Paschenko, S.; Utschig, L.; Lakshmi, K.; Thurnauer, M. *J. Am. Chem. Soc.* **2005**, *127*, 11910−11911.
(25) Poulsen, A. K.; Rompel, A.; McKenzie, C. J. *Angew. Chem., Int. Ed.* **2005**, *44*, 6916−6920.
(26) Wiechen, M.; Berends, H. M.; Kurz, P. *Dalton Trans.* **2012**, *41*, 21−31.
(27) Cady, C. W.; Crabtree, R. H.; Brudvig, G. W. *Coord. Chem. Rev.* **2008**, *252*, 444−455.
(28) Cady, C. W.; Shinopoulos, K. E.; Crabtree, R. H.; Brudvig, G. W. *Dalton Trans.* **2010**, *39*, 3985−3989.
(29) Tagore, R.; Chen, H. Y.; Crabtree, R. H.; Brudvig, G. W. *J. Am. Chem. Soc.* **2006**, *128*, 9457−9465.
(30) Wang, T.; Brudvig, G.; Batista, V. S. *J. Chem. Theory Comput.* **2010**, *6*, 755−760.
(31) Wang, T.; Brudvig, G. W.; Batista, V. S. *J. Chem. Theory Comput.* **2010**, *6*, 2395−2401.
(32) Luo, S.; Rivalta, I.; Batista, V.; Truhlar, D. G. *J. Phys. Chem. Lett.* **2011**, *2*, 2629−2633.
(33) Amin, M.; Vogt, L.; Vassiliev, S.; Rivalta, I.; Sultan, M. M.; Bruce, D.; Brudvig, G. W.; Batista, V. S.; Gunner, M. R. *J. Phys. Chem. B* **2013**, *117*, 6217−6226.
(34) Limburg, J.; Vrettos, J. S.; Liable-Sands, L. M.; Rheingold, A. L.; Crabtree, R. H.; Brudvig, G. W. *Science* **1999**, *283*, 1524−1527.
(35) Limburg, J.; Vrettos, J. S.; Chen, H. Y.; de Paula, J. C.; Crabtree, R. H.; Brudvig, G. W. *J. Am. Chem. Soc.* **2001**, *123*, 423−430.
(36) Yagi, M.; Narita, K. *J. Am. Chem. Soc.* **2004**, *126*, 8084−8085.
(37) Narita, K.; Kuwabara, T.; Sone, K.; Shimizu, K.-i.; Yagi, M. *J. Phys. Chem. B* **2006**, *110*, 23107−23114.
(38) Li, G.; Sproviero, E. M.; McNamara, W. R.; Snoeberger, R. C., III; Crabtree, R. H.; Brudvig, G. W.; Batista, V. S. *J. Phys. Chem. B* **2010**, *114*, 14214−14222.
(39) Li, G.; Sproviero, E. M.; Snoeberger, R. C., III; Iguchi, N.; Blakemore, J. D.; Crabtree, R. H.; Brudvig, G. W.; Batista, V. S. *Energy Environ. Sci.* **2009**, *2*, 230−238.
(40) McNamara, W. R.; Snoeberger, R. C.; Li, G.; Schleicher, J. M.; Cady, C. W.; Poyatos, M.; Schmuttenmaer, C. A.; Crabtree, R. H.; Brudvig, G. W.; Batista, V. S. *J. Am. Chem. Soc.* **2008**, *130*, 14329−14338.
(41) Busch, M.; Ahlberg, E.; Panas, I. *Phys. Chem. Chem. Phys.* **2011**, *13*, 15069−15076.
(42) Siegbahn, P.; Heiberg, A.; Roos, B. O.; Levy, B. *Phys. Scr.* **1980**, *21*, 323−327.
(43) Roos, B. O.; Taylor, P. R.; Sigbahn, P. E. M. *Chem. Phys.* **1980**, *48*, 157−173.
(44) Andersson, K.; Malmquvist, P.-Å.; Roos, B. O.; Sadlej, A. J.; Wolinski, K. *J. Phys. Chem.* **1990**, *94*, 5483−5488.
(45) Andersson, K.; Malmqvist, P.-Å.; Roos, B. r. O. *J. Chem. Phys.* **1992**, *96*, 1218−1226.
(46) Noodleman, L.; Davidson, E. R. *Chem. Phys.* **1986**, *109*, 131−143.
(47) Frisch, M. J.; Trucks, G. W.; Schlegel, H. B.; Scuseria, G. E.; Robb, M. A.; Cheeseman, J. R.; Scalmani, G.; Barone, V.; Mennucci, B.; Petersson, G. A.; Nakatsuji, H.; Caricato, M.; Li, X.; Hratchian, H. P.; Izmaylov, A. F.; Bloino, J.; Zheng, G.; Sonnenberg, J. L.; Hada, M.; Ehara, M.; Toyota, K.; Fukuda, R.; Hasegawa, J.; Ishida, M.; Nakajima, T.; Honda, Y.; Kitao, O.; Nakai, H.; Vreven, T.; Montgomery, J. A., Jr.; Peralta, J. E.; Ogliaro, F.; Bearpark, M.; Heyd, J. J.; Brothers, E.; Kudin, K. N.; Staroverov, V. N.; Kobayashi, R.; Normand, J.; Raghavachari, K.; Rendell, A.; Burant, J. C.; Iyengar, S. S.; Tomasi, J.; Cossi, M.; Rega, N.; Millam, J. M.; Klene, M.; Knox, J. E.; Cross, J. B.; Bakken, V.; Adamo, C.; Jaramillo, J.; Gomperts, R.; Stratmann, R. E.; Yazyev, O.; Austin, A. J.; Cammi, R.; Pomelli, C.; Ochterski, J. W.; Martin, R. L.; Morokuma, K.; Zakrzewski, V. G.; Voth, G. A.; Salvador, P.; Dannenberg, J. J.; Dapprich, S.; Daniels, A. D.; Farkas, Ö.; Foresman, J. B.; Ortiz, J. V.; Cioslowski, J.; Fox, D. J. *Gaussian 09*, Revision C; Gaussian, Inc.: Wallingford, CT, 2009.
(48) Becke, A. D. *J. Chem. Phys.* **1993**, *98*, 5648−5652.
(49) Lee, C.; Yang, W.; Parr, R. G. *Phys. Rev. B* **1988**, *37*, 785−789.
(50) Hay, P. J.; Wadt, W. R. *J. Chem. Phys.* **1985**, *82*, 299−310.
(51) Dunning, T. H. *J. Chem. Phys.* **1989**, *90*, 1007−1023.
(52) Kendall, R. A.; Dunning, T. H.; Harrison, R. J. *J. Chem. Phys.* **1992**, *96*, 6796−6806.
(53) Woon, D. E.; Dunning, T. H. *J. Chem. Phys.* **1993**, *98*, 1358−1371.
(54) Milikisiyants, S.; Chatterjee, R.; Lakshmi, K. V. *J. Phys. Chem. B* **2011**, *115*, 12220−12229.
(55) Campbell, M. L.; Waite, B. A. *J. Chem. Educ.* **1990**, *67*, 386−388.
(56) Chen, Z.; Concepcion, J. J.; Hu, X.; Yang, W.; Hoertz, P. G.; Meyer, T. J. *Proc. Natl. Acad. Sci. U.S.A.* **2010**, *107*, 7225−7229.
(57) Fecenko, C. J.; Thorp, H. H.; Meyer, T. J. *J. Am. Chem. Soc.* **2007**, *129*, 15098−15099.
(58) Surendranath, Y.; Kanan, M. W.; Nocera, D. G. *J. Am. Chem. Soc.* **2010**, *132*, 16501−16509.
(59) Costentin, C.; Donati, L.; Robert, M. *Chem.—Eur. J.* **2009**, *15*, 785−792.
(60) Cramer, C. J.; Tolman, W. B.; Theopold, K. H.; Rheingold, A. L. *Proc. Natl. Acad. Sci. U.S.A.* **2003**, *100*, 3635−3640.

DOI: 10.1021/acscatal.5b00048
ACS Catal. 2015, 5, 2384−2390